BNL-HET-03/10
FSU-HEP-2003-0513
UB-HET-03/04
hep-ph/0305282

ASSOCIATED HIGGS BOSON PRODUCTION WITH HEAVY QUARKS

S. DAWSON[1], L. H. ORR[2], L. REINA[3,a], D. WACKEROTH[4]
[1]*Physics Department, Brookhaven National Laboratory, Upton, NY 11973, USA*
[2]*Department of Physics and Astronomy, University of Rochester, Rochester, NY 14627, USA*
[3]*Physics Department, Florida State University, Tallahassee, FL 32306-4350, USA*
[4]*Department of Physics, SUNY at Buffalo, Buffalo, NY 14260, USA*

The production of a Higgs boson in association with a pair of $t\bar{t}$ quarks will play a very important role at both hadron and lepton colliders. We review the status of theoretical predictions and their relevance to Higgs boson studies, with particular emphasis on the recently calculated NLO QCD corrections to the inclusive cross section for $p\bar{p}, pp \to t\bar{t}h$. We conclude by briefly discussing the case of exclusive $b\bar{b}h$ production and the potential of this process in revealing signals of new physics beyond the Standard Model.

1 Introduction

Present and future colliders will play a crucial role in exploring the nature of the electroweak symmetry breaking and its relation to the origin of fermion masses. The discovery of a Higgs boson is therefore among the most important goals of both the Tevatron and the Large Hadron Collider (LHC). Had such a particle to be discovered, a high energy Linear Collider (LC) will be able to identify it unambiguously.

The present lower bounds on the Higgs boson mass from direct searches at LEP2 are $M_h > 114.4$ GeV (at 95% CL) [1] for the Standard Model (SM) Higgs boson (h), and $M_{h^0} > 91.0$ GeV and $M_{A^0} > 91.9$ GeV (at 95% CL, $0.5 < \tan\beta < 2.4$ excluded) [1] for the light scalar (h^0) and pseudoscalar (A^0) Higgs bosons of the minimal supersymmetric standard model (MSSM). At the same time, global SM fits to electroweak precision data imply $M_h < 211$ GeV (at 95% CL) [2], while the MSSM requires the existence of a scalar Higgs boson lighter than about 130 GeV. The possibility of a Higgs boson discovery in the mass range near 115-130 GeV thus seems increasingly likely.

In this context the associated production of a Higgs boson with a pair of $t\bar{t}$ quarks is kinematically accessible, has a very distinctive signature, and can give the only handle on a direct measurement of the top quark Yukawa coupling, perhaps the most crucial coupling in exploring the origin of fermion masses.

Observing $p\bar{p} \to t\bar{t}h$ at the Tevatron ($\sqrt{s}=2$ TeV) will require very high luminosity [3] and will probably be at the edge of the machine capabilities. On the other hand, if $M_h \leq 130$ GeV, $pp \to t\bar{t}h$ is an important discovery channel for a SM-like Higgs boson at the LHC ($\sqrt{s}=14$ TeV) [4,5,6,7].

[a] Talk presented by L. Reina. at the XXXVIIIth Rencontres de Moriond, Les Arcs, March 15-22 2003

Given the statistics expected at the LHC, $pp \to t\bar{t}h$, with $h \to b\bar{b}, \tau^+\tau^-, W^+W^-, \gamma\gamma$ will also be instrumental to the determination of the couplings of a discovered Higgs boson [6,8,9,10]. Several analyses show that precisions of the order of 10-15% on the measurement of the top quark Yukawa coupling can be obtained with integrated luminosities of 100 fb^{-1} per detector. Morever, the combined measurements of $pp \to t\bar{t}h$ with $h \to b\bar{b}$ and $h \to \tau^+\tau^-$ could provide the only model independent determination of the ratio of the bottom quark to the τ lepton Yukawa couplings [9].

At a LC, the top quark Yukawa coupling can be measured in a model independent way via $e^+e^- \to t\bar{t}h$. The inclusive cross section for $e^+e^- \to t\bar{t}h$ (and $b\bar{b}h$) has been calculated including the first order of QCD corrections, both in the SM and in the MSSM [16,17], and the theoretical uncertainty is reduced in this case to less than 10%. However, the precision of the measurement is severely limited by the machine center of mass energy. Dedicated studies show that [11], at the optimal center of mass energy of $\sqrt{s}\simeq 800$ GeV, integrated luminosities of 1000 fb^{-1} will allow to determine the top quark Yukawa coupling at the 5% level, for $M_h = 120$ GeV. However, at a center of mass energy of $\sqrt{s} = 500$ GeV the $e^+e^- \to t\bar{t}h$ event rate is tiny and, for the same range of Higgs masses and integrated luminosity, a LC will initially measure the top Yukawa coupling with precisions of at best 20% [11,12]. Given this intrinsic limitation, the role played by the LHC and, in this context, by the associated production of a Higgs boson with a pair of $t\bar{t}$ quarks becomes even more important.

In view of its phenomenological relevance, a lot of effort has been recently invested in improving the stability of the theoretical predictions for the hadronic inclusive total cross section for $p\bar{p}, pp \to t\bar{t}h$. Since the tree level or Leading Order (LO) cross section is affected by a very large renormalization and factorization scale dependence, the first order of QCD corrections have been calculated and the Next-to-Leading (NLO) cross section, for a SM Higgs boson, has been obtained independently by two groups [13,14,15]. The NLO cross section has a drastically reduced renormalization and factorization scale dependence, of the order of 15% as opposed to the initial 100% uncertainty of the LO cross section, and leads to increased confidence in predictions based on these results.

The calculation of the NLO corrections to the hadronic process $p\bar{p}, pp \to t\bar{t}h$ presents challenging technical difficulties, ranging from virtual pentagon diagrams with several massive internal and external particles to real gluon and quark emission in the presence of infrared singularities. A general overview of the techniques developed and employed in our calculation are presented in Section 2, and the corresponding results are illustrated in Section 3. We conclude with a brief outlook in Section 4.

2 QCD corrections to $t\bar{t}h$ production at the Tevatron and the LHC

The inclusive total cross section for $pp \to t\bar{t}h$ at $\mathcal{O}(\alpha_s^3)$ can be written as:

$$\sigma_{NLO}(p\overset{(-)}{p} \to t\bar{t}h) = \sum_{ij} \frac{1}{1+\delta_{ij}} \int dx_1 dx_2 \left[\mathcal{F}_i^p(x_1,\mu)\mathcal{F}_j^{p(\bar{p})}(x_2,\mu)\hat{\sigma}_{NLO}^{ij}(x_1,x_2,\mu) + (1 \leftrightarrow 2)\right] \quad , \tag{1}$$

where $\mathcal{F}_i^{p(\bar{p})}$ are the NLO parton distribution functions (PDFs) for parton i in a (anti)proton, defined at a generic factorization scale $\mu_f = \mu$, and $\hat{\sigma}_{NLO}^{ij}$ is the $\mathcal{O}(\alpha_s^3)$ parton-level total cross section for incoming partons i and j, made of the channels $q\bar{q}, gg \to t\bar{t}h$ and $(q,\bar{q})g \to t\bar{t}h(q,\bar{q})$, and renormalized at an arbitrary scale μ_r which we also take to be $\mu_r = \mu$. We note that the effect of varying the renormalization and factorization scales independently has been investigated and found to be negligible. The partonic center of mass energy squared, s, is given in terms of the hadronic center of mass energy squared, s_H, by $s = x_1 x_2 s_H$. At the Tevatron center of mass energy the cross section is entirely dominated by the $q\bar{q}$ initial state and the results presented in Section 3 are obtained by including only $q\bar{q} \to t\bar{t}h$ at the parton level. At the LHC center of mass energy the cross section is dominated by the gg initial state, but the other contributions cannot be neglected and are included in our calculation.

We write the NLO parton-level total cross section $\hat{\sigma}^{ij}_{NLO}(x_1, x_2, \mu)$ as:

$$\hat{\sigma}^{ij}_{NLO}(x_1, x_2, \mu) \equiv \hat{\sigma}^{ij}_{LO}(x_1, x_2, \mu) + \delta\hat{\sigma}^{ij}_{NLO}(x_1, x_2, \mu) \ , \tag{2}$$

where $\hat{\sigma}^{ij}_{LO}(x_1, x_2, \mu)$ is the $\mathcal{O}(\alpha_s^2)$ Born cross section, and $\delta\hat{\sigma}^{ij}_{NLO}(x_1, x_2, \mu)$ consists of the $\mathcal{O}(\alpha_s)$ corrections to the Born cross sections for $gg, q\bar{q} \to t\bar{t}h$ and of the tree level $(q,\bar{q})g \to t\bar{t}h(q,\bar{q})$ processes, including the effects of mass factorization. $\delta\hat{\sigma}^{ij}_{NLO}(x_1, x_2, \mu)$ can be written as the sum of two terms:

$$\begin{aligned} \delta\hat{\sigma}^{ij}_{NLO}(x_1, x_2, \mu) &= \int d(PS_3)\overline{\sum}|\mathcal{A}_{virt}(ij \to t\bar{t}h)|^2 + \int d(PS_4)\overline{\sum}|\mathcal{A}_{real}(ij \to t\bar{t}h + l)|^2 \\ &\equiv \hat{\sigma}^{ij}_{virt}(x_1, x_2, \mu) + \hat{\sigma}^{ij}_{real}(x_1, x_2, \mu) \ , \end{aligned} \tag{3}$$

where $|\mathcal{A}_{virt}(ij \to t\bar{t}h)|^2$ and $|\mathcal{A}_{real}(ij \to t\bar{t}h + l)|^2$ (for $ij = q\bar{q}, gg$ and $l = g$, or $ij = qg, \bar{q}g$ and $l = q, \bar{q}$) are respectively the $\mathcal{O}(\alpha_s^3)$ terms of the squared matrix elements for the $ij \to t\bar{t}h$ and $ij \to t\bar{t}h + l$ processes, and $\overline{\sum}$ indicates that they have been averaged over the initial state degrees of freedom and summed over the final state ones. Moreover, $d(PS_3)$ and $d(PS_4)$ in Eq. (3) denote the integration over the corresponding three and four-particle phase spaces respectively. The first term in Eq. (3) represents the contribution of the virtual one gluon corrections to $q\bar{q} \to t\bar{t}h$ and $gg \to t\bar{t}h$, while the second one is due to the real one gluon and real one quark/antiquark emission, i.e. $q\bar{q}, gg \to t\bar{t}h + g$ and $qg(\bar{q}g) \to t\bar{t}h + q(\bar{q})$.

The $\mathcal{O}(\alpha_s)$ virtual and real corrections to $q\bar{q} \to t\bar{t}h$ and $gg \to t\bar{t}h$ have been discussed in detail in Refs.[14,15] and we will highlight in the following only the most challenging tasks.

2.1 Virtual correction

The calculation of the $\mathcal{O}(\alpha_s)$ virtual corrections to $q\bar{q}, gg \to t\bar{t}h$ proceeds by reducing each virtual diagram to a linear combination of tensor and scalar integrals, which may contain both ultraviolet (UV) and infrared (IR) divergences. Tensor integrals are further reduced in terms of scalar integrals[18]. The finite scalar integrals are evaluated by using the method described in Ref.[19] and cross checked with the FF package[20]. The scalar integrals that exhibit UV and/or IR divergences are calculated analytically. Both the UV and IR divergences are extracted by using dimensional regularization in $d = 4 - 2\epsilon$ dimensions. The UV divergences are then removed by introducing a suitable set of counterterms, as described in detail in Refs.[14,15]. The remaining IR divergences are cancelled by the analogous singularities in the soft and collinear part of the real gluon emission cross section.

The most difficult integrals arise from the IR-divergent pentagon diagrams with several massive particles. The pentagon scalar and tensor Feynman integrals originating from these diagrams present either analytical (scalar) or numerical (tensor) challenges. We have calculated the pentagon scalar integrals as linear combinations of scalar box integrals using the method of Ref.[21], and cross checked them using the techniques of Ref.[19]. Pentagon tensor integrals can give rise to numerical instabilities due to the dependence on inverse powers of the Gram determinant (GD), GD$=\det(p_i \cdot p_j)$ for p_i and p_j external momenta, which vanishes at the boundaries of phase space when two momenta become degenerate. These are spurious divergences, which cause serious numerical difficulties. To overcome this problem we have calculated and cross checked the pentagon tensor integrals in two ways: numerically, by isolating the numerical instabilities and extrapolating from the numerically safe to the numerically unsafe region using various techniques; and analytically, by reducing them to a numerically stable form.

2.2 Real correction

In computing the $\mathcal{O}(\alpha_s)$ real corrections to $q\bar{q}, gg \to t\bar{t}h$ and $(q,\bar{q}g \to t\bar{t}h + (q,\bar{q})$ it is crucial to isolate the IR divergent regions of phase space and extract the corresponding singularities analytically. We achieve this by using the phase space slicing (PSS) method, in both the double[22] and single[23,24] cutoff approaches. In both approaches the IR region of the $t\bar{t}h+g$ phase space where the emitted gluon cannot be resolved is defined as the region where the gluon kinematic invariants:

$$s_{ig} = 2p_i \cdot p_g = 2E_i E_g (1 - \beta_i \cos\theta_{ig}) \tag{4}$$

become small. Here p_i is the momentum of an external (anti)quark or gluon (with energy E_i), $\beta_i = \sqrt{1 - m_i^2/E_i^2}$, p_g is the momentum of the radiated final state gluon ((anti)quark) (with energy E_g), and θ_{ig} is the angle between $\vec{p}_i$ and $\vec{p}_g$. In the IR region the cross section is calculated analytically and the resulting IR divergences, both soft and collinear, are cancelled, after mass factorization, against the corresponding divergences from the $\mathcal{O}(\alpha_s)$ virtual corrections.

The single cutoff PSS technique defines the IR region as that where

$$s_{ig} < s_{min} \ , \tag{5}$$

for an arbitrarily small cutoff s_{min}. The two cut-off PSS method introduces two arbitrary parameters, δ_s and δ_c, to separately define the IR soft and IR collinear regions according to:

$$\begin{aligned} &E_g < \frac{\delta_s \sqrt{s}}{2} \quad \text{soft region} \ , \\ &(1 - \cos\theta_{ig}) < \delta_c \quad \text{collinear region} \ . \end{aligned} \tag{6}$$

In both methods, the real contribution to the NLO cross section is computed analytically below the cutoffs and numerically above the cutoffs, and the final result is independent of these arbitrary parameters. With this respect, it is crucial to study the behavior of σ_{NLO} in a region where the cutoff(s) are small enough to justify the analytical calculations of the IR divergent contributions to the real cross section, but not so small as to cause numerical instabilities.

3 Results for $t\bar{t}h$ production at hadron colliders

The impact of NLO QCD corrections on the tree level cross section is summarized in Figs. 1-4 for both the Tevatron and the LHC. Results for σ_{LO} are obtained using the 1-loop evolution of $\alpha_s(\mu)$ and CTEQ4L parton distribution functions[25], while results for σ_{NLO} are obtained using the 2-loop evolution of $\alpha_s(\mu)$ and CTEQ4M parton distribution functions, with $\alpha_s^{NLO}(M_Z) = 0.116$.

Figs. 1 and 3 illustrate the renormalization/factorization scale dependence of σ_{LO} and σ_{NLO} at the Tevatron and the LHC. In both cases the NLO cross section shows a drastic reduction of the scale dependence with respect to the lowest order prediction. Figs. 2 and 4 complement this information by illustrating the dependence of the LO and NLO cross sections on the Higgs boson mass at both the Tevatron and the LHC.

The overall uncertainty on the theoretical prediction, including the errors coming from parton distribution functions and the top quark mass (which we take to be $m_t = 174$ GeV), is reduced to only 15-20%, as opposed to the 100-200% uncertainty of the LO cross section. Including NLO QCD corrections decreases (Tevatron) or increases (LHC) the LO cross section for a broad range of commonly used renormalization and factorization scales (obtained *e.g.* by varying μ by a factor of two around $\mu = \mu_0$), and over the entire Higgs boson mass range considered in our study. This can be summarized by defining a K-factor, $K = \sigma_{NLO}/\sigma_{LO}$, which is however affected by the same strong scale dependence as the LO cross section, as well as by the choice of PDFs. When using CTEQ4 PDFs the K-factor corresponding to Figs. 1-4 is around $0.7-0.95$ at the Tevatron and $1.2-1.4$ at the LHC, for most choices of scales and Higgs boson mass.

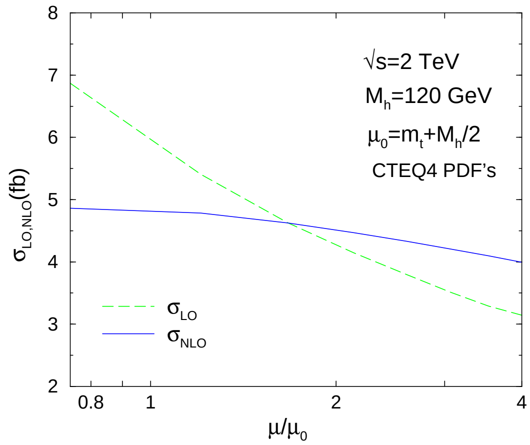

Figure 1: Dependence of $\sigma_{LO,NLO}(p\bar{p}\to t\bar{t}h)$ on the renormalization/factorization scale μ, at $\sqrt{s_H}=$ 2 TeV, for $M_h=120$ GeV.

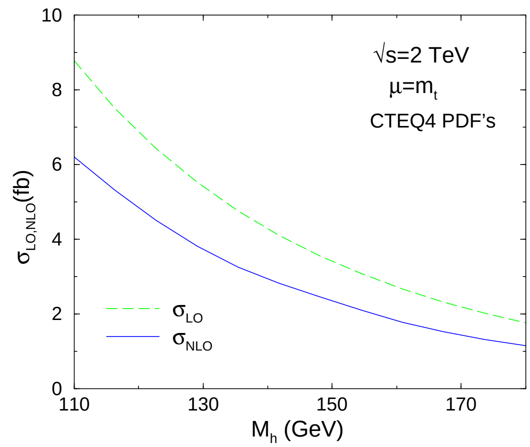

Figure 2: $\sigma_{NLO}(p\bar{p}\to t\bar{t}h)$ and $\sigma_{LO}(pp\to t\bar{t}h)$ as functions of M_h, at $\sqrt{s_H}=2$ TeV, for $\mu=m_t$.

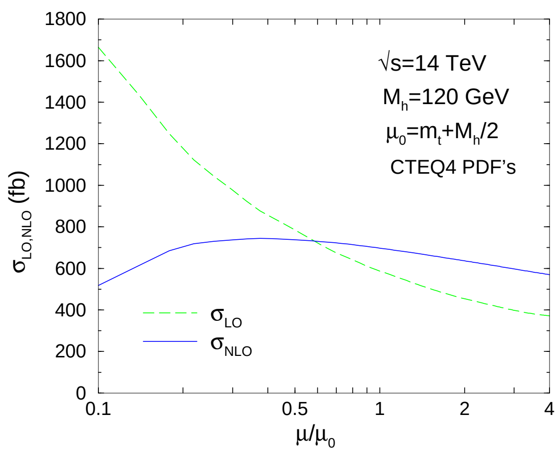

Figure 3: Dependence of $\sigma_{LO,NLO}(pp\to t\bar{t}h)$ on the renormalization/factorization scale μ, at $\sqrt{s_H}=$ 14 TeV, for $M_h=120$ GeV.

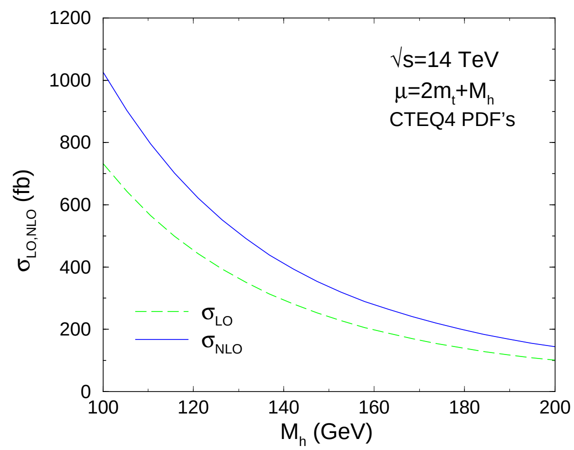

Figure 4: $\sigma_{NLO}(pp\to t\bar{t}h)$ and $\sigma_{LO}(pp\to t\bar{t}h)$ as functions of M_h, at $\sqrt{s_H}=14$ TeV, for $\mu=2m_t+M_h$.

4 Outlook

The techniques developed to calculate the NLO cross section for $p\bar{p},pp\to t\bar{t}h$ can now be applied to the study of the associated production of $b\bar{b}h$. The inclusive cross section for $b\bar{b}h$ production receives contributions from $b\bar{b}\to h$, $bg\to bh$, and $gg\to b\bar{b}h$, in order of decreasing cross section ($q\bar{q}\to b\bar{b}h$ is negligible at both the Tevatron and the LHC). On the other hand, the exclusive cross section, corresponding to the experimental situation when both final state b quarks are tagged, receives contributions from $gg\to b\bar{b}h$ only and can be directly calculated, including NLO corrections, from the corresponding results for $gg\to t\bar{t}h$. In spite of the smaller cross section, the exclusive process is experimentally very interesting since it corresponds to a well defined maesurement, where final state b jets are isolated via cuts on the transverse momentum of the b and $\bar{b}$ quarks. The cross section for $gg\to b\bar{b}h$ is negligible in the SM and the detection of a Higgs boson in this channel would unambiguously signal the presence of new physics responsible for an anomalously large bottom quark Yukawa coupling, like the MSSM. This could actually be a unique opportunity within the kinematical reach of the Tevatron.

Acknowledgments

The work of S.D. (L.H.O., L.R.) is supported in part by the U.S. Department of Energy under grant DE-AC02-76CH00016 (DE-FG-02-91ER40685, DE-FG02-97ER41022). L.R. thanks the National Science Foundation for supporting her participation to this meeting.

References

1. LHWG Note/2002-03, July 2002; Note/2001-04, July 2001.
2. LEPEWWG/2003-01, April 2003.
3. J. Goldstein, J. Incandela, S. Parke, D. Rainwater, D. Stuart, and C. Hill, *Phys. Rev. Lett.*, 86:1694–1697, 2001.
4. ATLAS Collaboration (1999), CERN/LHCC/99-15.
5. E. Richter-Was and M. Sapinski, *Acta Phys. Polon.*, B30:1001–1040, 1999.
6. M. Beneke et al. (2000), hep-ph/0003033.
7. V. Drollinger, T. Muller, and D. Denegri (2001), hep-ph/0111312.
8. D. Zeppenfeld, R. Kinnunen, A. Nikitenko, and E. Richter-Was, *Phys. Rev.*, D62:013009, 2000. D. Zeppenfeld (2002), hep-ph/0203123.
9. A. Belyaev and L. Reina, *JHEP*, 08:041, 2002.
10. F. Maltoni, D. Rainwater, and S. Willenbrock, *Phys. Rev.*, D66:034022, 2002.
11. A. Juste and G. Merino (1999), hep-ph/9910301.
12. H. Baer, S. Dawson, and L. Reina, *Phys. Rev.*, D61:013002, 2000.
13. W. Beenakker, S. Dittmaier, M. Krämer, B. Plümper, M. Spira, and P. M. Zerwas, *Phys. Rev. Lett.*, 87:201805, 2001; *Nucl. Phys.*, B653:151–203, 2003.
14. L. Reina and S. Dawson, *Phys. Rev. Lett.*, 87:201804, 2001.
    L. Reina, S. Dawson, and D. Wackeroth. *Phys. Rev.*, D65:053017, 2002.
15. S. Dawson, L. H. Orr, L. Reina, and D. Wackeroth, *Phys. Rev.*, D67:071503, 2003.
    S. Dawson, C. Jackson, L. H. Orr, L. Reina, and D. Wackeroth (2003), hep-ph/0305087.
16. S. Dittmaier, M. Kramer, Y. Liao, M. Spira, and P. M. Zerwas, *Phys. Lett.*, B441:383–388, 1998; *Phys. Lett.*, B478:247–254, 2000.
17. S. Dawson and L. Reina, *Phys. Rev.*, D59:054012, 1999; *Phys. Rev.*, D60:015003, 1999.
18. G. Passarino and M. J. G. Veltman, *Nucl. Phys.*, B160:151, 1979.
19. A. Denner, *Fortschr. Phys.*, 41:307–420, 1993.
20. G. J. van Oldenborgh and J. A. M. Vermaseren, *Z. Phys.*, C46:425–438, 1990.
21. Z. Bern, L. J. Dixon, and D. A. Kosower, *Phys. Lett.*, B302:299–308, 1993, Erratum-ibid. **B318**, 649 (1993); *Nucl. Phys.*, B412:751–816, 1994.
22. B. W. Harris and J. F. Owens, *Phys. Rev.*, D65:094032, 2002.
23. W. T. Giele and E. W. N. Glover, *Phys. Rev.*, D46:1980–2010, 1992.
    W. T. Giele, E. W. N. Glover, and D. A. Kosower, *Nucl. Phys.*, B403:633–670, 1993.
24. S. Keller and E. Laenen, *Phys. Rev.*, D59:114004, 1999.
25. H. L. Lai et al., *Phys. Rev.*, D55:1280–1296, 1997.